JOURNAL OF MATERIALS SCIENCE 31 (1996) 2131–2138

Thermal shock behaviour of a coarse grain porous alumina

Part I *Temperature field determination*

F. MIGNARD, C. OLAGNON, G. FANTOZZI, P. CHANTRENNE*, M. RAYNAUD*
*Laboratoire GEMPPM, URA CNRS 341, bât. 502 and *Laboratoire CETHIL, URA CNRS 1372, bât. 404, INSA de Lyon, 20 bd. A. Einstein, 69621 Villeurbanne Cedex, France*

An apparatus of thermal shock by air cooling in which experiments can be precisely modelled is presented. The different physical parameters have been measured as a function of the temperature. The heat transfer coefficient has also been determined by two methods, on a copper specimen and directly on the alumina thermal shock specimen. A precise knowledge of the transient temperature field is therefore available.

1. Introduction

Ceramics are brittle and generally present a low thermal conductivity. This makes them sensitive to thermal stresses induced by transient or steady heat transfer. Thermal shock properties are therefore very important and have been intensively studied these last years, both on theoretical and experimental bases.

The analysis of the thermal shock properties was first conducted by Kingery [1] using a thermoelastic analysis. It is based on the evaluation of the maximum surface stress during a thermal shock characterized by the temperature difference ΔT. The degradation is assumed to occur when this stress reaches the fracture strength of the ceramic. The severity of the thermal shock, i.e. the heat transfer kinetic can be taken into account through the introduction of the Biot number. An alternative analysis based on a fracture criteria was further introduced by Hasselman [2]. Defects are supposed to exist in the material and in the analysis their stability is studied. This analysis shows an important point of the thermal shock which is the stability of pre-existing large defects, which can explain the good thermal shock resistance of refractories. Several thermal shock parameters derived [3, 4] from these two analyses have been proposed. These parameters can be used as guides for material selection but cannot give fine prediction since they are based on global properties of materials and general thermal shock conditions [5].

Modified analyses have been first proposed by Evans and Charles [6] in order to introduce a stress intensity factor instead of the stress, which brings the advantage of requiring the toughness rather than the strength for the failure criteria. This analysis has been refined by improving the description of the temperature field and the stress field [7, 8]. The fracture criteria has also been improved by conducting a more refined stress intensity factor analysis [9] and later by taking into account the temperature dependence of the material characteristics [10, 11].

However, the theoretical description being complex, many different thermal shock experiments have been used [12]. In any case these experiments consist in simulating a thermal stress. They can be classified into two types: decreasing or increasing thermal shock. The classification is of importance since it leads to different transient stress states and to different working temperatures. The decreasing temperature test consists in cooling a specimen by a given fluid which drives the cooling rate. The most extensively used systems are the water quench test [2] or quenching in air or in oil [13] or in fluidized bed or by contact [14]. The water quenching presents the advantage of leading to high stress but the surface thermal exchange is relatively difficult to predict because of the water boiling. Rising temperature tests are based on different experiments using rapid heating by laser beam [15], electrode discharge [16], hot gas [17], mirror furnace [18], or by plasma jet [19].

In the case of quenching experiments, that are easy to conduct, the major modelling difficulty is the determination of the surface thermal exchange. It is especially critical in experiments where the quenching medium is boiling, such as water, or oil. The surface heat exchange coefficient is indeed strongly dependent of temperature and time. The case of cooling by jet air or gas is less critical since the dependence over temperature of the coefficient is much less significant. However, only sparse values of this coefficient have been proposed in the literature. Moreover, only average values are generally given and their measurements are therefore necessary for a fine model of a thermal shock experiment that can be extended to component prediction.

The purpose of this paper is to present an apparatus for thermal shock and thermal fatigue experiments that can be precisely modelled in order to infer data that can be used for prediction. For this purpose a detailed analysis of the transient temperature and stress field is conducted. In a first part, the different

0022–2461

parameters of the materials, have been measured as a function of the temperature. The surface thermal coefficient has also been measured for the different faces of the specimen. A calculation of the temperature distribution has been achieved by finite difference and finite element methods with a one and two-dimensional model.

2. Experimental procedure

2.1. Material

A highly pure (> 99.5%) commercial porous alumina recommended for its very good resistance to thermal shock, was used in the present experiments. The average grain size is quoted by the manufacturers to be in a range of 50–100 μm. A total porosity of 15% was measured by Archimedes' method, with an average pore size of 2 μm determined by mercury porosimeter. Parallelipedic flexure test specimens ($4 \times 6 \times 40\ mm^3$) were used as ground for thermal shock tests.

2.2. Thermal shock device

The specimen was vertically fixed on a sample holder that could be alternatively moved between a cooling and a heating system. The heating system consisted in an electric furnace (up to 1000 °C). The cooling system consisted in two pulsed air nozzles at room temperature as shown in Fig. 1. The room temperature air flow was regulated in pressure and volume flow rate and applied to the two largest faces of the specimen. The bottom part of the sample holder played the role of a wave guide that transmits the acoustic emission to a piezoelectric transducer placed in the cold part of the device. The thermal shock procedure and all acoustic data collections were automatically monitored by a computer. The acoustic data were recorded during the first six cooling seconds. The fine calibration of the device allowed us to obtain the instants of acoustic peaks on a time scale calibrated on the onset of cooling. Acoustic emission peak appearances indicated the quenching time corresponding to the onset of unstable crack propagation. The thermal shock cycle consisted in holding the specimen to various stabilized temperatures during 10 min and cooling them for 6 s. The cooling time was of 6 s because it was shown that no further degradation occurred after that time. It should be noted that the sample acoustic emission measurements could also permit to stop the cycling for thermal fatigue experiments (when the acoustic activity reached a fixed threshold).

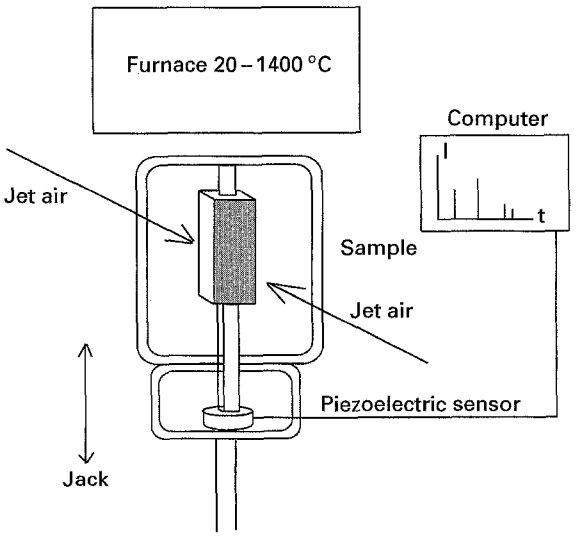

Figure 1 Thermal shock device.

2.3. Modelling

The temperature field within the specimen was determined by solving the transient non-linear heat diffusion equation (thermophysical parameters were taken as a function of temperature). The heat transfer by conduction within the material is given by

$$\rho(T)C_p(T)\frac{\partial T}{\partial t} = \frac{\partial}{\partial x}\left(k(T)\frac{\partial T}{\partial x}\right) + \frac{\partial}{\partial y}\left(k(T)\frac{\partial T}{\partial y}\right) \quad (1)$$

Where ρ is the density, C_p the specific heat at constant pressure, k the thermal conductivity and T the temperature. The surface heat exchange including convective and radiative exchanges can be represented by

$$-k(T)\frac{\partial T}{\partial n} = h(T)(T_{surface} - T_{r.t.}) \quad (2)$$

Where h is the surface heat transfer coefficient, n the outward surface normal, $T_{r.t.}$ the temperature of the cooling system and $T_{surface}$ the temperature at the surface of the body. Analytical solutions are well known for linear equations in monodimensional problems, but most practical problems require numerical calculations. In the present work finite differences and finite elements were used to solve the non-linear system of equations for the one- and two-dimensional problems, respectively.

3. Thermophysical properties of the alumina

Resolution of the heat diffusion equation (Equation 1) required the knowledge of the following thermophysical properties: thermal conductivity, specific heat and density. These properties have been studied as a function of temperature. This is mostly useful for thermal air quench where the specimen temperature variation can be large. The thermal conductivity $k(T)$ was evaluated from

$$k(T) = \rho(T)C_p(T)\chi(T) \quad (3)$$

where ρ is the density, C_p the specific heat at constant pressure, and χ the thermal diffusivity. The evolution of the density was calculated from the following expression

$$\rho(T) = \rho_{r.t.}(1 - 3\alpha_L(T - T_{r.t.})) \quad (4)$$

where α_L is the coefficient of linear expansion which was measured with a dilatometer (Adamel DI22) having a fused silica holder in a range of temperature between 20 and 1000 °C in air. Experimental data of

the coefficient of linear expansion are fitted with Equation 5 and represented in Fig. 2.

$$\alpha_L(T) = 10^{-6}(3.28582 + 2.73664 \times 10^{-2} T - 4.8873 \times 10^{-5} T^2 + 3.454 \times 10^{-8} T^3 - 6.13 \times 10^{-12} T^4) \quad (5)$$

where α_L is expressed in $°C^{-1}$.

Thermal diffusivity of the alumina was measured by the laser-flash method (this work was done at Laboratoire de Science et Génie des Matériaux Métalliques, URA 159, Ecole des Mines de Nancy, France) from room temperature to 1000 °C by gradual steps of 50 °C in a N_2 atmosphere. No significant difference in measurements was observed for a decreasing temperature procedure. The samples (10 mm in diameter and 3 mm thick discs) were coated with a carbon film in order to give a complete absorption of the laser-flash in the material. Experimental data of the thermal diffusivity are fitted with Equation 6 and are also represented in Fig. 2

$$\chi(T) = \frac{1250}{T + 150} 10^{-6} \quad (6)$$

where χ is expressed in $m^2 s^{-1}$ and T in °C. Note that the thermal diffusivity shows a dramatic decrease with increasing temperature which justifies taking into account this temperature dependence for the calculations. The values for this alumina are also lower than that for a dense alumina [20] which shows the role of the porosity.

The specific heat data at constant pressure was collected from literature. Indeed, since C_p is an intensive property, it only depends on chemical and crystallographic nature of the material, but not on porosity. Considering the high purity of the alumina used in experiments, Equation 7 determined for a dense polycrystalline alumina by Furukawa and colleagues [21] was employed

$$C_p(T) = 1448.94 - 33.57 \times 10^{-3} T - \frac{200\,306.1416}{T + 273.16} \quad (7)$$

where C_p is expressed in J $Kg^{-1} °C^{-1}$ for a temperature range between 127 and 923 °C.

The thermal conductivity values calculated from Equation 3 are represented in Fig. 3. Note that there is

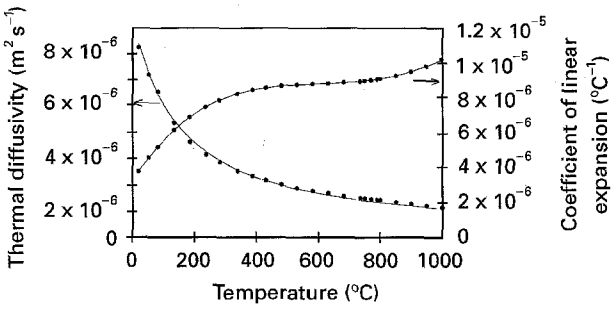

Figure 2 Temperature dependence of thermal diffusivity and coefficient of linear expansion of AL24 alumina. • experimental data; – fitted equation.

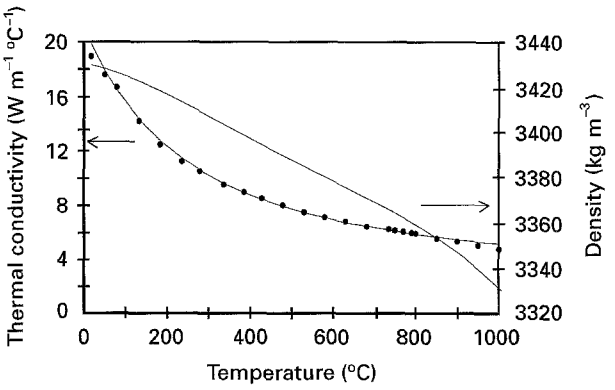

Figure 3 Temperature dependence of thermal conductivity and density of A124 alumina.

a significant decrease of thermal conductivity with increasing temperature which again shows that it is necessary to consider such a temperature dependence to predict the temperature field. Thermal conductivity values of the alumina AL24 are quite lower than those found for a dense alumina (35 $W m^{-1} °C^{-1}$ [22]). Although less significant than for other thermophysical properties, the temperature dependence of density was taken into account.

4. Surface heat transfer coefficient

4.1. Empirical relations

Because of the complicated nature of the flow-separation processes around the specimen, it is not possible to calculate analytically the average forced heat transfer coefficients in cross flow. However, correlations of experimental data allow the determination of the average heat transfer coefficient from the following dimensionless formula

$$Nu = C Re^n Pr^{\frac{1}{3}} \quad (8)$$

where Nu, Re, and Pr are the Nusselt, Reynolds and Prandtl numbers respectively. The fluid properties must be evaluated at the film temperature $T_f = (T_{surface} - T_{fluid})/2$. The constants C and n are given by Holman [23] for cross flow over various non-circular cylinders. However, the case of a rectangle cooled by forced convection over two opposite faces is not reported. The closest configuration is for the case of a square body cooled by a single impinging jet for which $C = 0.102$ and $n = 0.675$ when $5 \times 10^{+3} < Re < 10^{+5}$. The average heat transfer coefficient determined from this correlation is around 1000 W $m^{-2} °C^{-1}$, but the main problem is to determine the fluid velocity at the nozzle outlet, i.e. the uncertainty on Re is large. Correlation formulas were used by Tranchand [24] but the coefficient C had to be changed so as to obtain a reasonable agreement between the calculated and measurement specimen temperatures. Clearly, such a procedure is not satisfying. Herein, it has been decided to determine experimentally the heat transfer coefficients around the test specimen.

4.2. Experimental estimation methods

The estimation of the heat transfer coefficient, h, from transient temperature measurements is a difficult task. In the previous studies on thermal shock testing of ceramics, it has more or less been determined by trial and error [25, 26]. There are two main approaches that can be used to accurately estimate the heat transfer coefficient. The first one, called the lumped body approach is the most simple and has been used for measuring heat transfer coefficients and heat fluxes for a number of applications including determination of the boiling curve. A thermally lumped body is one in which the temperature is uniform but varies with time. The heat loss from the body surface results in a decrease in its internal energy, thus

$$\rho(T)C_p(T)V\frac{\partial T}{\partial t} = h(t)(T_{surface} - T_{r.t.})S_a \quad (9)$$

where S_a is the surface area for cooling and V is the volume. Such a simple heat conduction model yields reasonable temperature estimates when the following condition on the Biot number is met

$$\text{Biot} = \frac{h(V/S_a)}{k} < 0.1 \quad (10)$$

where the ratio V/S_a can be seen as the characteristic dimension of the solid. It shows that the internal thermal resistance is negligible compared to the external one, i.e. it is valid for a small body with a high thermal conductivity. By approximating the time derivative with finite differences, the solid temperature measurements allow the determination of the heat transfer coefficient at any time

$$h(t) = \rho(T^n)C_p(T^n)\frac{V}{S_a}\frac{T^{n+1} - T^n}{\Delta t}\frac{1}{T^n - T_{r.t,}} \quad (11)$$

where Δt is the time period between measurements and T^n represents the specimen temperature at time $n\Delta t$. This procedure is particularly simple to use, moreover, it is possible to estimate a time dependent heat transfer coefficient.

In the second approach, the interior temperature gradients are taken into account. The estimation of transient unknown boundary conditions from internal temperature measurements is commonly referred to as the inverse heat conduction problem (IHCP). The IHCP has extensively been studied over the last three decades with several textbooks entirely devoted to this problem [27, 28, 29]. The IHCP is an ill-posed problem, i.e. it is very sensitive to the random noise measurements. There are, however, many situations where it is impossible to place a sensor at the surface or where the accuracy of the surface measurements is seriously impaired by the presence of the sensor. Consequently, it is often preferable to accurately measure the temperature at interior location and to solve a tractable IHCP rather than to rely on inaccurate measurements. However, there are limitations such as the number of sensors and their locations for bi-dimensional problems. For a one-dimensional problem, it has been shown that the dimensionless time step based on the distance, E, between the surface and the sensor

$$\Delta t_i = \frac{\chi \cdot \Delta t}{E^2} \quad (12)$$

should be larger than 5×10^{-3}. The larger Δt_i, the easier the inversion. Several methods have especially been developed for the solution of the IHCP. Among these, the space marching finite differences methods are the most efficient [30, 31] but are limited to one-dimensional problems. The algorithm proposed by Raynaud and Bransier is shortly described herein for the special case where the sensor is placed on an insulated boundary. Central finite differences are used to approximate the one-dimensional heat conduction equation

$$\rho_i^n C_{p_i}^n \frac{T_i^{n+1} - T_i^{n-1}}{2\Delta t} = \frac{q_{i-1/2}^n - q_{i+1/2}^n}{\Delta x} \quad (13)$$

The discretization grid is shown in Fig. 4, T_i^n represents the temperature at the spatial node i and at the time step n (where i is a dummy variable which is equal to $1, 2, 3 \ldots, j-1, j$). For the IHCP, the sensitivity to the random measurement noise necessitates to introduce a specific step to ensure the stability of the algorithm

$$q_{i+1/2}^n = \frac{q_{i+1/2}^{n+1} + q_{i+1/2}^{n-1}}{2} \quad (14)$$

Then the approximation of the heat flux densities with central differences leads to an explicit relation for the unknown temperature

$$T_{i-1}^n = T_i^n + \frac{\rho_i^n C_{p_i}^n \Delta x^2}{\lambda_{i-1/2}^n 2\Delta t}(T_i^{n+1} - T_i^{n-1}) + \frac{\lambda_{i+1/2}^{n+1}}{\lambda_{i-1/2}^n}\left(\frac{T_{i+1}^{n+1} - T_i^{n+1}}{2}\right) + \frac{\lambda_{i+1/2}^{n-1}}{\lambda_{i-1/2}^n}\left(\frac{T_{i+1}^{n-1} - T_i^{n-1}}{2}\right) \quad (15)$$

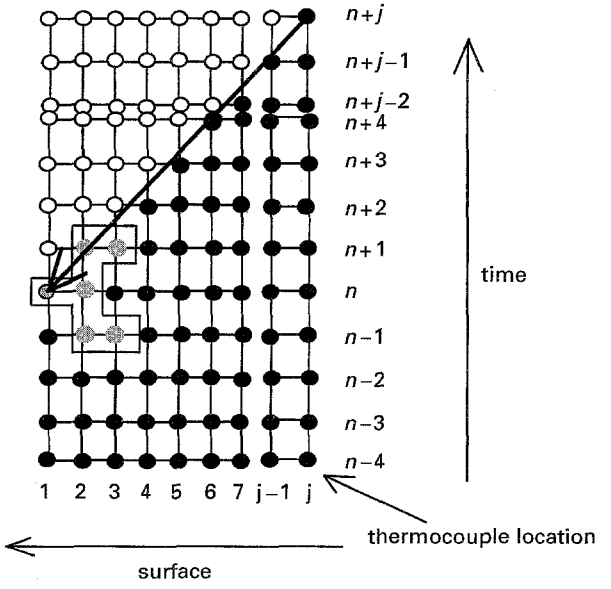

Figure 4 Thermal mesh: • calculated temperature; ○ temperature to be calculated at the next time step.

This relation is used as shown by the arrow in Fig. 4 to march forward in space and backward in time along the diagonal. A specific relation, that accounts for the insulated boundary at the measurement point, j, must be used for the first step. It is obtained from an energy balance on the half control volume placed on the adiabatic surface

$$\rho_j^n C_{p_j}^n \frac{\Delta x}{2} \frac{T_j^{n+1} - T_j^{n-1}}{2\Delta t} = q_{j-1/2}^n \qquad (16)$$

Central finite differences are also used to approximate $q_{j-1/2}^n$, thus

$$T_{j-1}^n = T_j^n + \frac{\Delta x^2}{4\Delta t} \frac{\rho_j^n C_{p_j}^n}{\lambda_{j-1/2}^n} (T_j^{n+1} - T_j^{n-1}) \qquad (17)$$

Once the surface temperature is determined, the surface heat flux density is calculated by writing the conservation of energy on the surface node similarly to Equation 16 [30]. The heat transfer coefficient is calculated at any time from Equation 2. Contrary to the direct problem, the time step must be large enough to have a tractable IHCP. The smaller the time step, the higher the sensitivity to measurement errors. For a given thermal diffusivity and sensor location, the criteria given before on the dimensionless time step can be used to evaluate the time step size. For this method, the spatial discretization must be chosen such that the Fourier modulus $M = a\Delta t/\Delta x^2$ be larger than 1 or 2. The larger M, the more stable the method. Further details can be found in [27, 30, 32].

4.3. Measurement and discussion

The objective is to estimate the overall heat transfer coefficient, h, around our test specimen by the two techniques described above. Overall, it means that it will account for both the convective and radiative heat exchanges. For given surface roughness and emissivity values h depends on the fluid flow around the specimen and on the radiative exchange and is thus independent of the material. The heat transfer coefficient can therefore be estimated with any material. In order to use the lumped body technique, a material with the following properties is required: (i) thermophysical properties precisely known and high thermal conductivity such that the Biot number be lower than 0.1; (ii) high resistance to thermal shock in order to prevent degradation; (iii) easy to machine in order to insert thermocouples correctly. For this purpose a high purity (99.9%) electrolytic copper was selected. Thermophysical properties of the copper specimen were indeed well known [33, 34]. The specimens must have nearly the same dimensions than those used for thermal shock tests so as to obtain a similar flow field. With these conditions the Biot number was about 4.5×10^{-2}, which allowed us to use the lumped body analysis. A 0.25 mm K-type sheathed and grounded thermocouple (to enhance time response), was longitudinally positioned in the middle of the specimen (Fig. 5). The voltage delivered by the thermocouple was collected every 6 ms by a data acquisition system (Keithley 500 A connected to a computer) during the

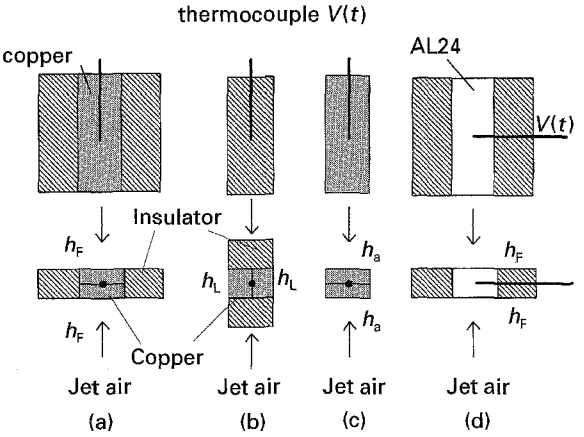

Figure 5 Different quenching conditions of a copper specimen.

thermal shock tests (which is compatible with the response time of the thermocouple). This permitted us to measure the evolution of the average temperature in the copper specimen as a function of cooling time $T(t)$. The surface heat transfer coefficient, h, is calculated from Equation 11. In order to estimate the local heat transfer coefficients, three various quenching conditions were tested (Fig. 5). The first one corresponded to a specimen which was thermally shocked by frontal faces (Fig. 5a). These unidirectional cooling conditions were carried out by protecting the lateral faces of the copper sample with an insulating refractory ceramic. The frontal heat transfer coefficient h_F was measured and calculated in this way. The second quenching conditions were also unidirectional, but the frontal faces instead of the lateral faces were protected by a refractory ceramic (Fig. 5b), which gave the lateral heat transfer coefficient, h_L. Finally, a copper specimen without any refractory protection permitted to measure the average surface heat coefficient h_a (considering the whole surface of the specimen), and to confirm that refractory protection had not affected air flow conditions (Fig. 5c). Moreover for all of these measurements, the upper and lower parts of the copper specimens were also insulated with the refractory material, preventing heat exchanges through these sides. Different measurements corresponding to different initial temperatures were conducted for a cooling time of 6 s.

The frontal surface heat transfer coefficient estimates are represented in Fig. 6. Note that the frontal heat transfer coefficient is independent of the temperature, showing that the radiative losses are small compared to the convective ones. The mean value of h_F calculated with the lumped model is $h_F = 590 \pm 45\ \mathrm{W\,m^{-2}\,°C^{-1}}$. The confidence interval has been calculated by taking into account the uncertainty in the thermal physical properties and the thermocouple location. Note also that the divergences near the time origin ($t \approx 0$ and $T \approx T_{ini}$), is due to the singularity of Equation 11 at $t = 0$. Only measurements on the plateau should therefore be considered. The h_F values evaluated by the space marching method from the same temperature measurements are also represented in Fig. 6. In this case the mean

h_F value is around $640 \pm 80\ W m^{-2} °C^{-1}$. Lateral heat transfer coefficient data calculated by the two methods are both represented in Fig. 7. h_L can also be considered as independent of the temperature. From these tests a mean value of $h_L = 550 \pm 45\ W m^{-2} °C^{-1}$ (lumped analysis) and of $h_L = 600 \pm 80\ W m^{-2} °C^{-1}$ (inverse method), i.e., slightly lower than for h_F, are found. It is remarkable that the lateral faces which are not directly exposed to compressed air flow, are nearly as much cooled as the frontal faces.

The average surface heat transfer coefficient h_a is shown in Fig. 8. In this case the heat conduction model being bi-dimensional, the space marching method cannot be used. The calculations have therefore been only conducted with the lumped model which is still a valid approach. A good reproducibility of the h_a data, with a mean value of $h_a = 590 \pm 45\ W m^{-2} °C^{-1}$ is observed. Assuming that the air flows for the different test configurations are similar, the following relation obtained from the conservation of energy principle should be satisfied

$$h_a S_a = h_F S_F + h_L S_L \quad (18)$$

For the above tests, it is verified within 3%.

In order to confirm the validity of the results with the copper specimen, some experiments were conducted on alumina samples (AL24 grade). For this purpose a hole was drilled (0.6 mm in diameter and 3 mm depth) in the middle of a lateral face of an alumina specimen. The objective, as shown by Fig. 5d, is to evaluate the frontal surface heat transfer coefficient. With alumina samples the Biot number is equal to 0.13 which indicates that the lumped body model cannot be used. The frontal heat transfer coefficient has only been estimated with the space marching method taking into account the alumina thermal properties variations. The h_F values evaluated in these conditions are represented in Fig. 9 with a mean value of $710 \pm 100\ W m^{-2} °C^{-1}$. It is 10% higher than for the copper sample but the two results are in good agreement if one considers the confidence intervals. The experimental uncertainties are larger for the experiments done with the alumina specimens. There are several reasons for these uncertainties. First, owing to the Biot number there is a temperature gradient within the specimen. Since the thermocouple size is significant compared to the specimen size, the measurement does not precisely indicate the centre temperature. A second cause of error is due to the low thermal conductivity of the alumina specimen. The conduction losses by the thermocouple may then not be negligible. This effect is all the more pronounced since the thermocouple is embedded on the side of the specimen at a depth of 3 mm (Fig. 5d). Such an error leads to a higher value of the surface heat transfer coefficient which is the case here. Finally, even if the copper results indicated that the radiative heat transfer was small compared to the convective one, a difference in the emissivities of the two materials can lead to such a small difference. However, it can be assumed that the

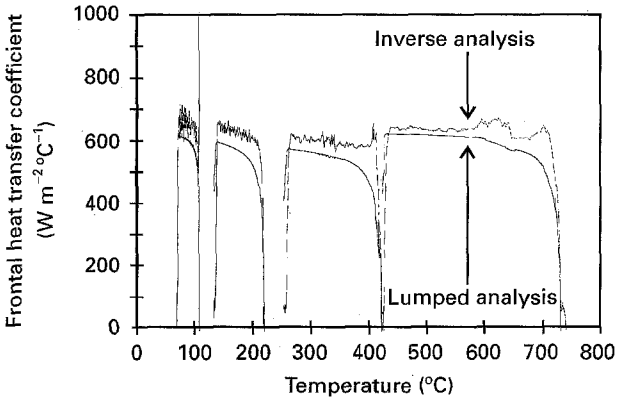

Figure 6 Frontal heat transfer coefficient, h_F, determined from experiment 5a.

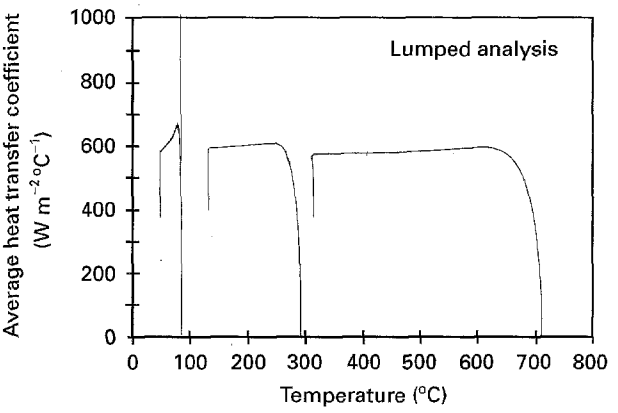

Figure 8 Average heat transfer coefficient, h_a, determined from experiment 5c.

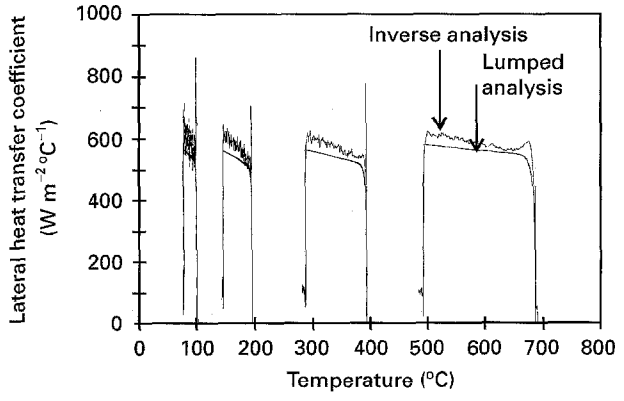

Figure 7 Lateral heat transfer coefficient, h_L, determined from experiment 5b.

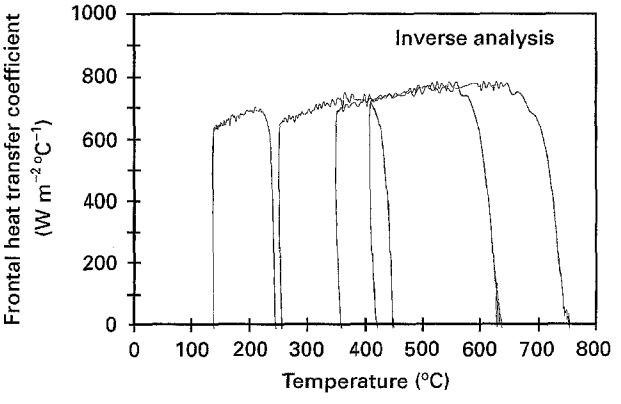

Figure 9 Frontal surface heat coefficient, h_F, evaluated from an alumina specimen.

convective heat transfer coefficient does not depend on the material.

The measurement conducted on the copper specimen is to be preferred since the temperature measurements are more accurate and the calculations are easier to conduct. The lumped body analysis appears to be an elegant and precise method for measuring the heat transfer coefficient. Such a method should be used whenever possible. Aside from the heat transfer coefficient value, this study showed that despite the two impinging jets, the cooling was similar on each face of the specimen. Thus even with a shape ratio of 2/3, the specimen temperature field will be highly bi-dimensional.

5. Temperature field within the specimen during thermal shock

The bi-dimensional cooling model defined by Equations 1 and 2 with frontal and lateral heat exchange defined by h_F and h_L (Fig. 10) is used to study the thermal shock tests of alumina AL24. From the previous results an average value of 600 $W m^{-2} °C^{-1}$ for the surface heat transfer coefficients was adopted. The evolution of the temperature field during the cooling cycle has been calculated with a finite elements code. The temperature dependence of the thermophysical properties was measured and the mesh was fine enough to obtain mesh-independent results. The temperature field of an alumina specimen thermally shocked with a 682 °C initial temperature difference is represented in Fig. 11 after 700 ms of cooling

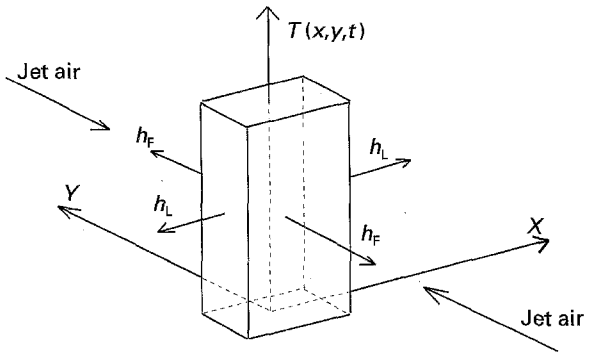

Figure 10 Thermal shock model of simulation.

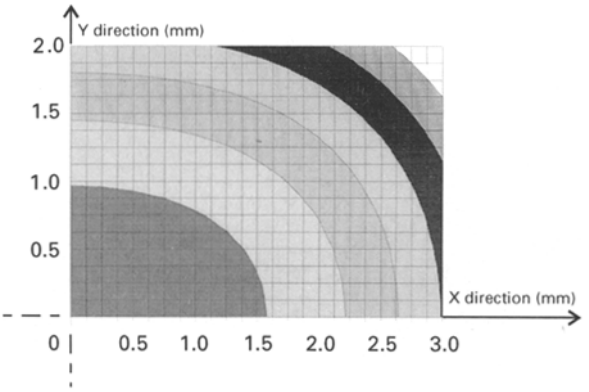

Figure 11 Temperature field within an alumina specimen: $T(x, y)$. Temperatures (°C) □ 580–595; ▩ 595–610; ■ 610–625; ▩ 625–640; ▩ 640–655; ▩ 655–670; ▩ 670–685.

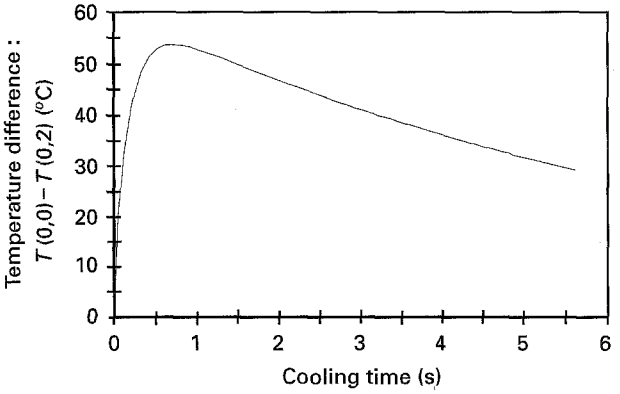

Figure 12 Temperature difference between the core and the surface of an alumina specimen during thermal shock testing.

time. Clearly the temperature field is bi-dimensional. Fig. 12 shows the variation of the temperature difference between the core and the centre surface of the specimen as a function of the cooling time. Note that this temperature difference increases up to a maximum value of 55 °C after 700 ms of cooling and decreases thereafter.

6. Conclusions

An apparatus of thermal shock by air cooling has been presented. The bi-dimensional transient temperature field was calculated with a finite elements method. The thermal diffusivity, the thermal conductivity and the coefficient of thermal expansion were independently measured as a function of temperature. Special care was also given to estimate the thermal boundary conditions, i.e. the surface heat transfer coefficients. They were precisely estimated from separate tests by two different methods. Within the thermal shock studies, it is, to our knowledge, the first time that independent experiments have been carried out to determine both the heat transfer coefficient and the thermophysical material properties.

It has been shown that the determination with a copper specimen which allowed us to use a lumped thermal model was accurate and simple. The results were confirmed on an alumina specimen. It showed, for these thermal shock test conditions, that the heat transfer coefficient does not depend on the specimen material. The lumped model could be used to estimate the cooling rate of any thermal shock test. These different measurements and theoretical analyses permit the precise determination of the transient temperature field within the specimen at any location. This kind of thermal analysis is necessary to predict the transient stress field and the thermal shock damage evaluation that will be published in Part II of this study.

Acknowledgement

The authors wish to acknowledge Dr R. Rezakhanlou and the Material Research Division of Electricité de France (EDF) for their financial support and their interest in this work.

References

1. W. D. KINGERY, *J. Amer. Ceram. Soc.* **38** (1955) 3.
2. D. P. H. HASSELMAN, *ibid.* **52** (1969) 600.
3. *Idem., Ceramurgia Int.* **4** (1978) 147.
4. *Idem., Mater. Sci. Eng.* **71** (1985) 251.
5. D. LEWIS, *J. Amer. Ceram. Soc.* **11–12** (1980) 713.
6. A. G. EVANS and E. A. CHARLES, *ibid.* **60** (1977) 22.
7. S. SATO, H. AWAJI and H. AKUZAWA, *Carbon* **16** (1978) 103.
8. C. SCHUBERT, H. A. BAHR and H. J. WEISS, *ibid.* **24** (1986) 21.
9. G. A. SCHNEIDER, *Ceram. Int.* **17** (1991) 325.
10. PH. PEIGNE, C. OLAGNON, G. FANTOZZI and P. PESNEAU, *Revue des composites et nouveaux matériaux* **1** (1991) 141.
11. PH. PEIGNE, PhD Thesis, INSA Lyon (1991).
12. J. C. GLANDUS and P. BOCH, *Interceram* **5** (1984) 33.
13. A. M. SIMONNEAU, PhD Thesis, Limoges University, France (1989).
14. W. P. ROGERS and A. F. EMERY, *J. Mater. Sci.* **27** (1992) 146.
15. G. KIRCHOFF, in "Thermal shock and thermal fatigue behaviour of advanced ceramics", edited by G. Schneider and G. Petzow, NATO ASI Series (Kluwer Academic Publishers, The Netherlands, 1993) p. 245.
16. S. SATO, Y. IMAMURA, A. KURUMADA, K. KAWAMATA, R. ISHIDA and H. AWAJI, *ibid.* p. 253.
17. G. C. WEI and J. WALSH, *J. Am. Ceram. Soc.* **72** (1989) 1286.
18. G. A. SCHNEIDER and G. PETZOW, *J. Amer. Ceram. Soc.* **74** (1991) 98.
19. J. LAMON and D. PHERSON, *ibid.* **74** (1991) 1188.
20. W. A. PLUMMER, D. E. CAMPBELL and A. A. COMSTOCK, in "Alumina as a ceramic material" (The American Ceramic Society, Inc., Colombus, OH, 1970).
21. G. T. FURUKAWA, in "Alumina as a ceramic material" (The American Ceramic Society, Inc., Colombus, OH, 1970).
22. Y. S. TOULOUKIAN, R.W. POWELL, C. Y. HO, and P. G. KLEMENS, "Thermophysical properties of materials, vol. 2, Thermal conductivity, nonmetallic solids" (IFI/Plenum, New York – Washington, 1970).
23. J. P. HOLMAN, "Heat transfer", 6th Edn (McGraw Hill, New York, 1986).
24. V. TRANCHAND, Thesis, Université de Limoges, November (1993).
25. T. NISHIKAWA, T. GAO, M. HIBI and M. TAKATSU, *J. Mater. Sci.* **29** (1994) 213.
26. A. GAUDON, Thesis, Université Paul Sabatier, Toulouse, December (1993).
27. J. V. BECK, B. BLACKWELL and C. ST CLAIR, "Inverse heat conduction, ill-posed problems" (Wiley Interscience, New York, 1985).
28. E. HENSEL, "Inverse theory and applications for engineers" (Prentice Hall, Englewood Cliffs, NJ, 1991).
29. D. MURIO, "The mollification method and the numerical solution of ill-posed problems" (Wiley Interscience, New York, 1993).
30. M. RAYNAUD and J. BRANSIERA, *Numerical Heat Transfer* **9** (1986) 27.
31. M. RAYNAUD and J. V. BECK, *J. Heat Transfer* **110** (1988) 30.
32. M. RAYNAUD and J. BRANSIER, in 8th International Heat Transfer Conference, Vol. 2, San Francisco, USA, 1986, p. 603.
33. Y. S. TOULOUKIAN, R. W. POWELL, C. Y. HO, and P. G. KLEMENS, "Thermophysical properties of materials, Vol. 1, Thermal conductivity, metallic elements and alloys" (IFI/Plenum, New York – Washington, 1970).
34. Y. S. TOULOUKIAN and E. H. BUYCO, "Thermophysical properties of materials, Vol. 4, Specific heat, metallic elements and alloys" (IFI/Plenum, New York – Washington, 1970).

Received 4 October 1994
and accepted 9 November 1995